https://doi.org/10.3311/PPch.38379

Periodica Polytechnica Chemical Engineering, 68(4), pp. 523–530, 2024

Study of the Gap Parameters of Cement Mortar Specimens Based on X-ray Tomography

András Kovács[1*]

[1] Institute of Materials Engineering, Faculty of Engineering, University of Pannonia, Egyetem Street 10., H-8200 Veszprém, Hungary
[*] Corresponding author, e-mail: kovacs.andras@mk.uni-pannon.hu

Received: 22 September 2024, Accepted: 14 November 2024, Published online: 21 November 2024

Abstract

Concrete is one of the most widely used structural materials next to steel. This justifies a detailed study of the material structure to understand the influence of the production parameters on the properties of the concrete. The pore structure of concretes has a major influence on their practical use, as it impacts their resistance to environmental degradation (e.g., frost resistance). In the present study, I have investigated concrete and cement mortar specimens with different water-cement ratios using micro-CT (or micro X-ray tomography) to determine the pore structure and the pore gap parameters of the specimens. It can be concluded that with an increasing water-cement ratio the overall porosity of the samples and the number of large pores (1 mm^3) show a decreasing trend, in contrast, the gap parameter shows an enhancing trend. It can also be concluded that any pore-forming additives cause significant changes in the structure.

Keywords

concrete, w/c ratio, gap parameter, X-ray tomography, micro-CT

1 Introduction

Concrete, one of the most complex structural materials [1–4], is widely used in the construction of buildings and infrastructure developments. However, environmental influences are a serious stress that can lead to deterioration such as cracking, spalling, and reduced load-bearing capacity. These problems result in significant renovation costs, not to mention the loss of functionality during renovation.

In practical engineering applications, concrete is often exposed to severe environmental influences, especially where salt-freeze-thaw (S-F-T) cycles occur. Here the macroscale performance of concrete is closely related to changes in the internal pore structure. Therefore, in the past decades, several studies have aimed [5-8] to investigate the influence of water/cement (w/c) ratio and curing time on the evolution of pore structure and mechanical properties of cementitious materials, because knowledge of these influences can be used to control the final structure. It was found that the compressive strength decreased with increasing w/c ratio while the cement content had less effect. Shrinkage and water absorption elevated with increasing w/c ratio, or at cement content. Rahmani et al. [7] showed that concrete wear resistance improved by 42% and concrete porosity decreased to 13.1% by reducing the w/c ratio from 0.46 to 0.30 in concrete specimens prepared with nano silica. Li et al. [8] used ice particles instead of liquid water as mixing water to prepare cement pastes and concluded that total porosity is the main factor in determining the compressive strength of cement pastes with super low w/c ratios. Based on experimental results [9–13], different mathematical prediction and regression models have been constructed to clarify the relationship between porosity and strength. Zheng et al. [14] have conducted a comprehensive study on the effect of freeze-thaw (F-T) cycles of different salt solutions on concrete. They emphasized that pores with a volume between 0.1 and 1 mm^3 have the greatest impact on the general properties of the system. The damage results from a combination of chemical and physical processes, including corrosion initiated by salt ions and pressure generated by solutions freezing in pores [15, 16].

Recently micro-CT has become a popular technique and is widely used to investigate the microstructural properties of cementitious materials. Lorenzoni et al. [17] began investigating the internal damage characteristics

Cite this article as: Kovács, A. "Study of the Gap Parameters of Cement Mortar Specimens Based on X-ray Tomography", Periodica Polytechnica Chemical Engineering, 68(4), pp. 523–530, 2024. https://doi.org/10.3311/PPch.38379

of Portland cement hydration products using micro-CT in 1997. Since then, the application of micro-CT techniques in the field of cement and concrete research has increased dramatically. Initially, micro-CT was used to study the internal structure of cement, such as pore types (pores and cracks) [18], pore shapes [19–22], and pore networks [23, 24]. Statistical and morphological analyses based on micro-CT provide a novel insight into the microstructure of cement as they can contribute to realistic 3D geometry [25]. du Plessis and Boshoff [26] have provided a comprehensive summary of the diverse applications of micro-CT, highlighting that its potential has been further exploited over the last decade, especially with the development of quantitative analysis capabilities.

The development of micro-CT equipment has allowed researchers to more efficiently analyze internal structural changes under mechanical stresses [27–30]. However, the measurement capabilities are limited by the maximum resolution of micro-CT equipment. A solution to this problem is the high-resolution micro-CT measurement technique presented by Cnudde and Boone [31], which allows clearer images and more detailed information but requires advanced image processing techniques. Advanced image processing techniques have emerged, including the use of deep learning to segment cracks from pores [32, 33], the use of gray level co-occurrence matrix (GLCM) to study cracks [34, 35], quantitative analysis methods, such as fractal dimension and roundness values for the analysis of pores [36, 37], the use of digital volume correlation (DVC) analysis methods to study the dynamic process of concrete fracture [38], and the integration of other experimental methods such as maximum intensity projection (MIP) to obtain more accurate porosity measurements [39]. The pores within a sample can be divided into external and internal categories, based on location. Current micro-CT techniques focus primarily on the examination of internal pores or cracks, it is important to recognize that external pores and cracks are in contact with the external environment and also have a significant influence on the strength properties of the material [40].

Schock et al. [41] used micro-CT to examine a sample from a concrete bridge on a German motorway. The study showed that the distance between the nearest pores in the pore structure can be determined in three dimensions. This makes the method suitable for statistical analysis. However, the influence of e.g., production parameters on the pore structure of concrete, including the spacing factor, has not been investigated.

In the present study, using the VG Studio Max (2023.1) software [42], the porosity analyzer module can determine the distance between equivalent spheres per pore. The study aims to investigate the effect of w/c ratio and air-entraining additives on the pore structure, which are important for frost resistance, with special emphasis on the pore gap parameter. This parameter does not directly match the commonly used spacing factor but provides essential information on the nature of the pore structure of the samples. As reported in the literature, the structure of concrete samples was in most cases investigated, because these are the most relevant material systems for practical applications. Preliminary experiments have been carried out where concrete specimens have been tested, however, the samples contain a large volume of large granules, which makes it difficult to compare individual series. This refers to the volumes that at high resolution can be examined by micro-CT. To avoid this, cement mortar samples were investigated in this study.

2 Experimental

2.1 Sample preparation

CEM III/A 32.5N-MSR type cement was used for the experiment and mixed with a sand additive according to EN 196-1:2016 [43]. The standard [43] specifies a water-cement ratio of 0.5. The water-cement ratio has been changed in relation to this. In addition, it is important to note that in all the experiments, the amount of 450 g of cement fixed in the standard was maintained. The samples were placed in standard 4 × 4 × 16 cm mortar molds. w/c ratio of 0.3, 0.4, 0.5 and 0.6 was applied. For the w/c ratio of 0.3 and 0.4, it was necessary to use a superplasticizer (Sika Viscocrete Neu 5) at 1.5% and 0.5%. It was required to deviate from the mixing program for the samples containing 1.5% superplasticizer by more resting (5 min) and intermittent slow mixing, as intensive mixing caused a lot of macropores (lower weight in 4 × 4 × 16 cm mortar mold) due to foaming and loosening. In addition, at a w/c ratio of 0.5, parallel samples were prepared by adding Sika Aer air-entraining concrete admixture (Table 1). The samples were stored underwater for 28 days, then stored at room temperature for one year, thus specimens with a stable pore structure were tested.

2.2 Measurement methods

Nikon XT H 225 ST X-Ray Tomograph instrument was applied to perform the micro-CT scans. During the measurements, 190 kV accelerating voltage, and 110 μA beam

Table 1 The investigated cement mortar samples

Sample ID	Type of cement	w/c ratio	Flow additive	Air entraining concrete admixture
CIII 0.3/450	CEM III/A 32.5N-MSR	0.3	1.5	0
CIII 0.4/450	CEM III/A 32.5N-MSR	0.4	0.5	0
CIII 0.5/450	CEM III/A 32.5N-MSR	0.5	0	0
CIII 0.6/450	CEM III/A 32.5N-MSR	0.6	0	0
CIII 0.5/450/LP	CEM III/A 32.5N-MSR	0.5	0	0.2

current were used. For the scan, 1300 projections were acquired with 2 frames/projection, which meant ~21 GB file size. During the reconstruction, scatter reduction, noise reduction, median filter, and image processing were applied to enhance the quality of the scans. For segmentation, the surface detection algorithm was used, in which small clusters were removed by the contour healing algorithm and internal porosity was closed. The Material Region Growing algorithm was then used to determine the outer boundary of the body containing the pores, thus generating the region of interest (ROI) for the porosity analysis. Finally, using the thresholding procedure of the porosity analysis module, the porosity of the samples was determined. The analysis was performed using the VG Studio Max (2023.1) software [42] and its porosity analysis module. It is important to note that the algorithm takes the distance between spheres of equivalent diameters, which can mean negative values if the distance between cavities is less than the sum of the equivalent diameters (e.g., the pores are elongated). In the analysis, three ranges were defined. The first class contains values less than 0 mm, where the equivalent spheres overlap. The next is the range 0–0.22 mm, which is not greater than 0.22 mm as defined in the microscopic test standard MSZ EN 480-11:2006 [44], but without overlapping equivalent spheres. Since the scans were taken with a resolution of 0.02 mm (thus there may be an error of +/− 0.01 mm), this was considered by making the mean value 0.22 mm and setting the upper value at 0.23 mm. The third group is the group of pores with a gap parameter greater than 0.23 mm.

3 Results and analysis

3.1 Experiments

The experiments were carried out on cement mortar samples with different water-cement ratios (Table 1). Cement mortar samples of the standard 4 × 4 × 16 cm size were applied to make the samples with different w/c ratios comparable. For the preparation of the samples, a superplasticizer was added for the 0.3 and 0.4 w/c ratios, and air-entraining concrete admixture was added for the 0.5 w/c ratio sample for comparison.

3.2 Micro-CT scan and evaluations

Micro-CT scans were performed on 4 × 4 × 16 cm samples by longitudinal rotation. Due to the sample size, the voxel resolution was approximately 20 µm. To check the effect of the resolution, subsequently, 2 × 2 × 4 cm pieces were cut for three samples (CIII 0.3/450, CIII 0.5/450 as well as CIII 0.3/450 LP), increasing the voxel resolution to 15 µm. After scanning the samples, reconstruction and porosity analysis were performed on the reconstructed files after surface determination.

The test was performed on large (4 × 4 × 16 cm) samples at 600 × 600 × 600 voxels ROIs, and on smaller (2 × 2 × 4 cm) samples at 800 × 800 × 800 voxels, therefore the physical volumes were the same.

The software could detect pores smaller than 0.01 mm^3 for each size, i.e., the resolution was suitable for investigating the required pore size range.

Figs. 1 and 2 show the two-dimensional sections of the cement mortar samples after micro-CT analysis. In Figs. 1 and 2 the air pores are shown in black, the lighter grey

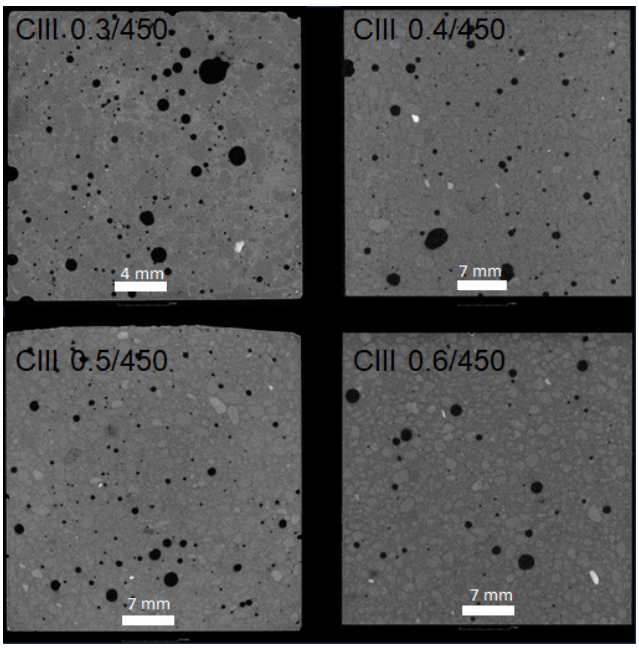

Fig. 1 2D micro-CT cross-section of scanned cement mortar samples with increasing w/c ratio (0.3, 0.4, 0.5, and 0. 6 respectively)

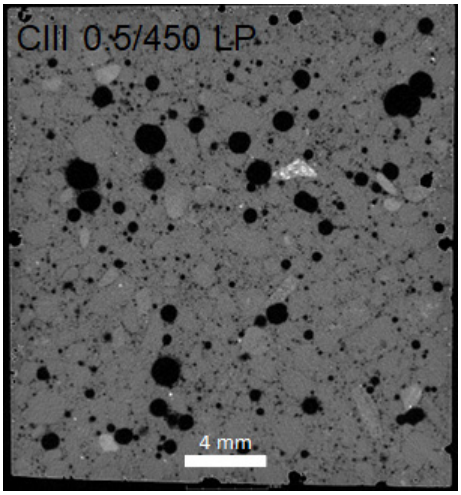

Fig. 2 2D micro-CT cross-section of scanned cement mortar sample with 0.5 w/c ratio containing air-entraining additive

areas indicate the cement paste phase and the lightest area is the standard sand additive. It can be seen that as the w/c ratio is increased, the number of pores with larger volumes (>1 mm^3) decreases, and regions that do not contain larger pores increase. In contrast, adding the air-entraining additive (Fig. 2) causes large pores that interconnect in a manner not seen in the other samples and causes significant quantity of fine porosity at the interface of additive particles and cement paste.

Significant differences in the pore structure can be observed by varying the w/c ratio, and in the case of the air-entraining additive, the nature of the pore structure changes. Figs. 3 and 4 show the results of the porosity analysis performed after the three-dimensional reconstruction. The volume of the cement paste and standard

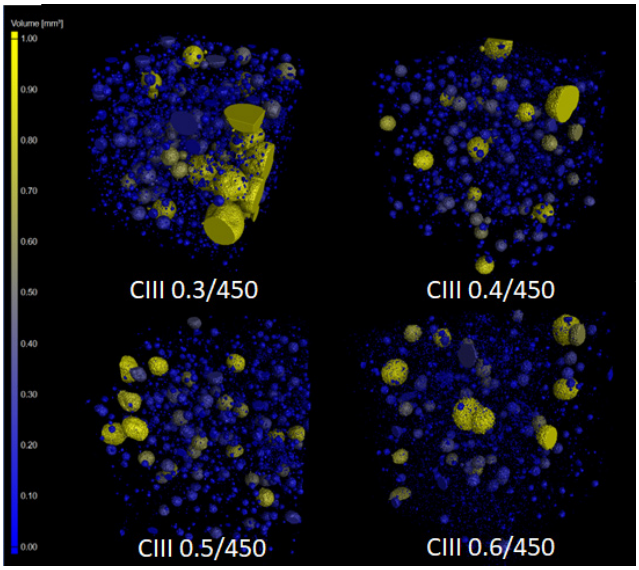

Fig. 3 3D visualization of porosity in the ROIs based on micro-CT scan of cement mortar samples with different w/c ratios

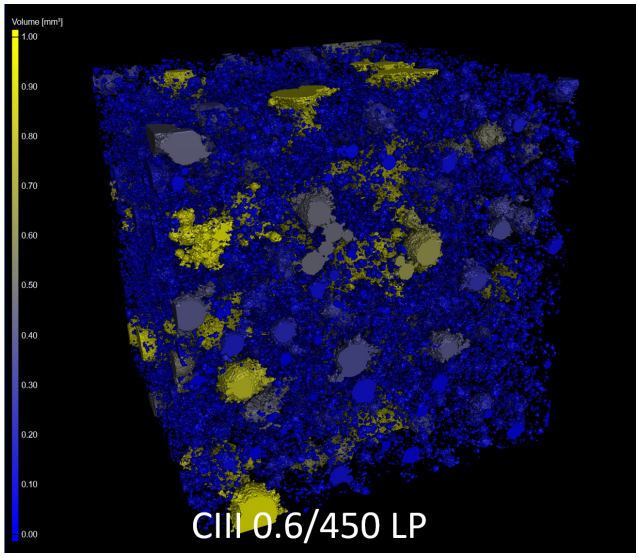

Fig. 4 3D visualization of porosity in the ROI based on micro-CT scan of cement mortar sample with 0.5 w/c ratio containing air-entraining additive

sand additive was made 100% transparent and the porosity was visualized by volume coloring. In the range 0–1 mm^3 the coloring is Virdis, meaning that the higher values are close to yellow one. The pores above 1 mm^3 are yellow-colored. It can be observed that the samples with w/c ratios of 0.3 and 0.4 have an approximately homogeneous fine porosity and contain spherical pores of larger size (>1 mm^3) that do not interconnect voids.

Due to their low water content, these samples contain a superplasticizer, which is likely to alter the plasticity of the cement paste to create these larger voids. In contrast, the samples with a w/c ratio of 0.5 and 0.6 have several voids, which do not contain a superplasticizer but have a higher water content. The sample with air-entraining additive in Fig. 4 shows significant homogeneously distributed porosity, consistent with the results in the two-dimensional section.

Figs. 5 and 6 show the pore size distributions of the samples. These were obtained using a logarithmic size scale. Differences are observed in the range of larger pore sizes, which are in accordance with the above.

Fig. 7 shows the gap parameter distribution plot generated from the numerical data of the test performed with the porosity analysis module of the VG Studio Max (2023.1) software [42]. Referred to Zheng et al. [14] the investigated lowest volume value is 0.01 mm^3. In the diagrams, the blue part shows the numerical ratio of gaps under 0 mm (in each other's spheres of equivalent diameter), the orange parts show the gaps between 0 mm and 0.23 mm, and the green parts show the higher gap parameter values. The

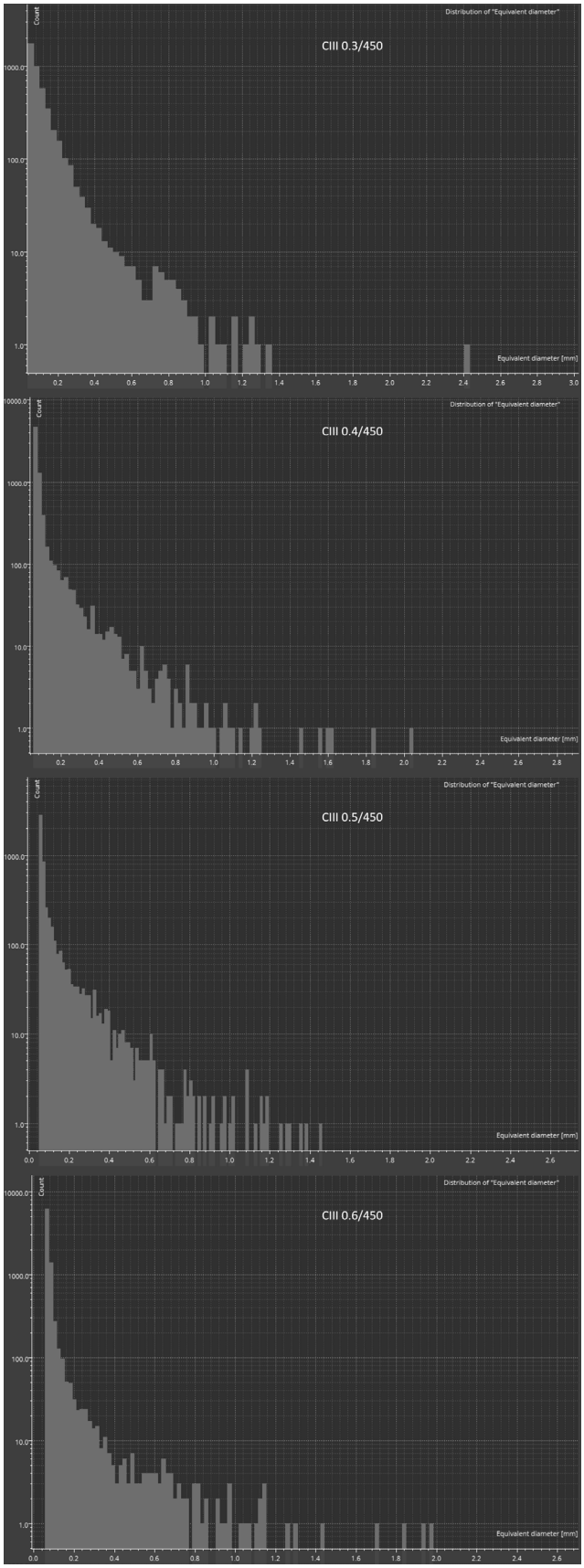

Fig. 5 Pore size distribution based on micro-CT scan of cement mortar samples with different w/c ratios

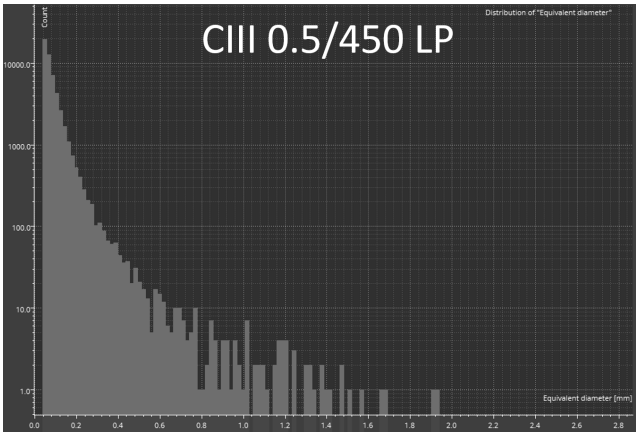

Fig. 6 Pore size distribution based on micro-CT scan of cement mortar sample with 0.5 w/c ratio containing air-entraining additive

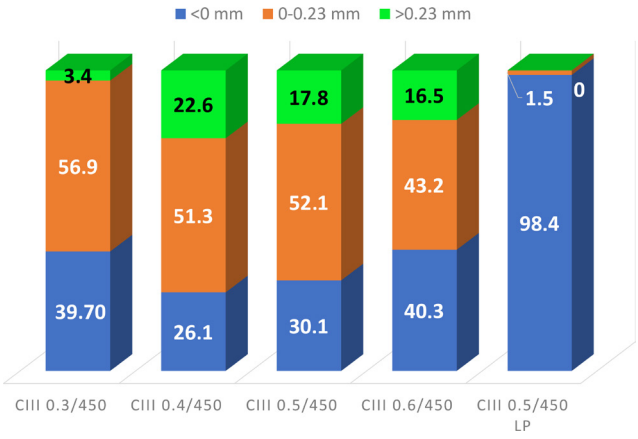

Fig. 7 Visualization of gap parameter distribution of cement mortar samples with increasing w/c ratio (0.3, 0.4, 0.5, and 0.6 respectively) and with 0.5 w/c ratio containing air-entraining additive classified by the gap parameter (<0 mm, 0–0.23 mm, and >0.23 mm)

gap parameter shows the distance of the two nearest pores' equivalent diameter spheres. This is a three-dimensional interpretation of the distance factor analysis using the microscopic technique. The purpose of this study is not to compare and mathematically match the two procedures with each other. However, the goal is to prove that changing the w/c ratio significantly affects the gap parameter, which is particularly important for cement mortars, i.e., concrete, in terms of resistance to environmental influences.

It is observed for a small number of pores, the associated gap parameter is higher than 0.23 mm for samples with a w/c ratio of 0.3 and samples containing an air-entraining additive. Therefore, it is important to investigate how much of the total pore volume is represented by pores with different gap parameters.

According to the diagrams presented for the numerical distribution of pores with different gap factors, the total volume of the distinct classes is shown in Fig. 8.

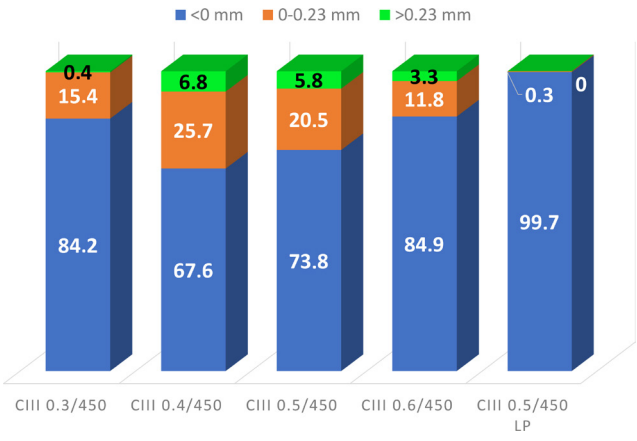

Fig. 8 Volume ratio visualization of cement mortar samples with increasing w/c ratio (0.3, 0.4, 0.5, and 0.6 respectively) and with 0.5 w/c ratio containing air-entraining additive classified by the gap parameter (<0 mm, 0–0.23 mm, and >0.23 mm)

In Fig. 8 the volumes corresponding to gap factors <0 mm, 0–0.23 mm as well as >0.23 mm are marked by blue, orange and green colors, respectively. Above the pore size distribution and the numerical distribution of pores with different gap parameters have been presented. However, the total volume of pores with different gap parameters is an important information (Table 2). The number of pores with a gap parameter of 0–0.23 mm and >0.23 mm and the total volume associated with these gap parameters peak at a w/c factor of 0.4 with increasing w/c ratio and then slowly decrease. It is important to highlight that the air-entraining additive causes a significant change in the pore structure as seen in the two-dimensional cross-section (Fig. 2).

Table 2 The total indication (void) volume/total volume ratios of cement mortar samples with increasing w/c ratios, and air-entraining additive content

Sample ID	Ratio indication volume/total volume (%)
CIII 0.3/450	7.96
CIII 0.4/450	2.21
CIII 0.5/450	2.31
CIII 0.6/450	1.76
CIII 0.5/450/LP	7.82

It strongly reduces the total volume of pores of higher gap parameters (> 0.23 mm). This information is essential for the use of the material system.

In the analysis, I also determined the total porosity of the different samples as a percentage by volume. The total porosity of the samples decreased with increasing w/c ratio but enhanced significantly with the addition of the air-entraining additive. The value of the CIII 0.5/450 LP sample is similar to that observed for the lowest (0.3) w/c ratio.

4 Conclusion

The study using micro-CT equipment investigated cement mortar samples with different w/c ratios. To ensure comparability and representativeness of the limited measurement volumes. It was found that with increasing w/c ratios the porosity decreases, the proportion of large pores (<1 mm^3) decreases, but the gap parameter increases in general. The number of pores with a gap parameter of 0–0.23 mm and >0.23 mm and the total volume associated with these gap parameters peak at a w/c factor of 0.4 with increasing w/c ratio and then slowly decrease. With the addition of an air-entraining additive, the pore structure changes abruptly, with several small (< 1 mm^3) pores with a significantly lower gap factor compared to a sample with the same w/c ratio. These results indicate that high S-F-T and F-T resistances can be expected by adding small w/c ratios or air-entraining additives.

Based on these results, mathematical harmonization of the distance factor determination by microscopic technique and the representative three-dimensional micro-CT method are required and the development of new measurement procedures are justified for future studies.

Acknowledgement

I would also like to acknowledge Dr. Ida Balczár Soósné, assistant professor, and Dr. Viktória Gável, researcher, for their professional support and good advice throughout the whole process of this study.

References

[1] Zhu, W., Feng, Q., Luo, Q., Yan, J., Lu, C. "Investigating the effect of polycarboxylate-ether based superplasticizer on the microstructure of cement paste during the setting process", Case Studies in Construction Materials, 16, e00999, 2022. https://doi.org/10.1016/j.cscm.2022.e00999

[2] Luo, Q., Zhang, X., Bai, Y., Yang, J., Geng, G. "Reduce the cost and embodied carbon of ultrahigh performance concrete using waste clay", Case Studies in Construction Materials, 19, e02670, 2023. https://doi.org/10.1016/j.cscm.2023.e02670

[3] Zhu, W., Feng, Q., Luo, Q., Bai, X., Chen, K., Lin, X. "Effect of a specific PCE superplasticizer on the initial dissolution and early hydration of Portland cement", Journal of Building Engineering, 46, 103786, 2022. https://doi.org/10.1016/j.jobe.2021.103786

[4] Zhu, W., Feng, Q., Luo, Q., Bai, X., Lin, X., Zhang, Z. "Effects of PCE on the Dispersion of Cement Particles and Initial Hydration", Materials, 14(12), 3195, 2021. https://doi.org/10.3390/ma14123195

[5] Schulze, J. "Influence of water-cement ratio and cement content on the properties of polymer-modified mortars", Cement and Concrete Research, 29(6), pp. 909–915, 1999. https://doi.org/10.1016/S0008-8846(99)00060-5

[6] Rao, G. A. "Role of water–binder ratio on the strength development in mortars incorporated with silica fume", Cement and Concrete Research, 31(3), pp. 443–447, 2001. https://doi.org/10.1016/S0008-8846(00)00500-7

[7] Rahmani, K., Rahmanzadeh, B., Piroti, S. "Experimental study of the effect of water-cement ratio on compressive strength, abrasion resistance, porosity and permeability of Nano silica concrete", Frattura ed Integrità Strutturale, 12(44), pp. 16–24, 2018. https://doi.org/10.3221/IGF-ESIS.44.02

[8] Li, L., Zhang, H., Guo, X., Zhou, X., Lu, L., Chen, M., Cheng, X. "Pore structure evolution and strength development of hardened cement paste with super low water-to-cement ratios", Construction and Building Materials, 227, 117108, 2019. https://doi.org/10.1016/j.conbuildmat.2019.117108

[9] Odler, I., Rößler, M. "Investigations on the relationship between porosity, structure and strength of hydrated Portland cement pastes. II. Effect of pore structure and of degree of hydration", Cement and Concrete Research, 15(3), pp. 401–410, 1985. https://doi.org/10.1016/0008-8846(85)90113-9

[10] Odler, I., Abdul-Maula, S. "Investigations on the relationship between porosity structure and strength of hydrated portland cement pastes III. Effect of clinker composition and gypsum addition", Cement and Concrete Research, 17(1), pp. 22–30, 1987. https://doi.org/10.1016/0008-8846(87)90054-8

[11] Li, Y.-X., Chen, Y.-M., Wei, J.-X., He, X.-Y., Zhang, H.-T., Zhang, W.-S. "A study on the relationship between porosity of the cement paste with mineral additives and compressive strength of mortar based on this paste", Cement and Concrete Research, 36(9), pp. 1740–1743, 2006. https://doi.org/10.1016/j.cemconres.2004.07.007

[12] Ozturk, A. U., Baradan, B. "A comparison study of porosity and compressive strength mathematical models with image analysis", Computational Materials Science, 43(4), pp. 974–979, 2008. https://doi.org/10.1016/j.commatsci.2008.02.011

[13] Ibrahim, A., Mahmoud, E., Yamin, M., Patibandla, V. C. "Experimental study on Portland cement pervious concrete mechanical and hydrological properties", Construction and Building Materials, 50, pp. 524–529, 2014. https://doi.org/10.1016/j.conbuildmat.2013.09.022

[14] Zheng, X., Liu, F., Luo, T., Duan, Y., Yi, Y., Hua, C. "Study on Durability and Pore Characteristics of Concrete under Salt Freezing Environment", Materials, 14(23), 7228, 2021. https://doi.org/10.3390/ma14237228

[15] Li, M., Zhang, Y., Wu, Z., Qian, C., Sun, W. "Effect of chloride salt and freeze-thaw cycling on the microstructure of concrete", Cement Wapno Beton, 18(2), pp. 74–80, 2013.

[16] Chen, S., Ren, J., Song, Y., Li, Q., Sun, J., Che, Y., Chen, J. "Salt Freeze-Thaw Damage Characteristics of Concrete based on Computed Tomography", Tehnički vjesnik, 26(6), pp. 1753–1763, 2019. https://doi.org/10.17559/TV-20190819080524

[17] Lorenzoni, R., Paciornik, S., Silva, F. A. "Characterization by microcomputed tomography of class G oil well cement paste exposed to elevated temperatures", Journal of Petroleum Science and Engineering, 175, pp. 896–904, 2019. https://doi.org/10.1016/j.petrol.2019.01.022

[18] Lu, S., Landis, E. N., Keane, D. T. "X-ray microtomographic studies of pore structure and permeability in Portland cement concrete", Materials and Structures, 39(6), pp. 611–620, 2006. https://doi.org/10.1617/s11527-006-9099-7

[19] Erdoğan, S. T., Nie, X., Stutzman, P. E., Garboczi, E. J. "Micrometer-scale 3-D shape characterization of eight cements: Particle shape and cement chemistry, and the effect of particle shape on laser diffraction particle size measurement", Cement and Concrete Research, 40(5), pp. 731–739, 2010. https://doi.org/10.1016/j.cemconres.2009.12.006

[20] Cepuritis, R., Garboczi, E. J., Ferraris, C. F., Jacobsen, S., Sørensen, B. E. "Measurement of particle size distribution and specific surface area for crushed concrete aggregate fines", Advanced Powder Technology, 28(3), pp. 706–720, 2017. https://doi.org/10.1016/j.apt.2016.11.018

[21] Ueda, T., Oki, T., Koyanaka, S. "Experimental analysis of mineral liberation and stereological bias based on X-ray computed tomography and artificial binary particles", Advanced Powder Technology, 29(3), pp. 462–470, 2018. https://doi.org/10.1016/j.apt.2017.11.004

[22] Nitka, M., Tejchman, J. "A three-dimensional meso-scale approach to concrete fracture based on combined DEM with X-ray μCT images", Cement and Concrete Research, 107, pp. 11–29, 2018. https://doi.org/10.1016/j.cemconres.2018.02.006

[23] Gallucci, E., Scrivener, K., Groso, A., Stampanoni, M., Margaritondo, G. "3D experimental investigation of the microstructure of cement pastes using synchrotron X-ray microtomography (μCT)", Cement and Concrete Research, 37(3), pp. 360–368, 2007. https://doi.org/10.1016/j.cemconres.2006.10.012

[24] Bossa, N., Chaurand, P., Vicente, J., Borschneck, D., Levard, C., Aguerre-Chariol, O., Rose, J. "Micro-and nano-X-ray computed-tomography: A step forward in the characterization of the pore network of a leached cement paste", Cement and Concrete Research, 67, pp. 138–147, 2015. https://doi.org/10.1016/j.cemconres.2014.08.007

[25] Yang, X., Kuru, E., Gingras, M., Iremonger, S. "CT-CFD integrated investigation into porosity and permeability of neat early-age well cement at downhole condition", Construction and Building Materials, 205, pp. 73–86, 2019. https://doi.org/10.1016/j.conbuildmat.2019.02.004

[26] du Plessis, A., Boshoff, W. P. "A review of X-ray computed tomography of concrete and asphalt construction materials", Construction and Building Materials, 199, pp. 637–651, 2019. https://doi.org/10.1016/j.conbuildmat.2018.12.049

[27] Tomoto, T., Moriyoshi, A., Takahashi, H., Kitagawa, H., Tsunekawa, M. "Damage to cement concrete pavements due to exposure to organic compounds in a cold region", Construction and Building Materials, 25(1), pp. 267–281, 2011. https://doi.org/10.1016/j.conbuildmat.2010.06.029

[28] Jivkov, A. P., Engelberg, D. L., Stein, R., Petkovski, M. "Pore space and brittle damage evolution in concrete", Engineering Fracture Mechanics, 110, pp. 378–395, 2013. https://doi.org/10.1016/j.engfracmech.2013.05.007

[29] Fan, Y., Luan, H. "Pore structure in concrete exposed to acid deposit", Construction and Building Materials, 49, pp. 407–416, 2013. https://doi.org/10.1016/j.conbuildmat.2013.08.075

[30] Xue, S., Meng, F., Zhang, P., Wang, J., Bao, J., He, L. "Influence of substrate moisture conditions on microstructure of repair mortar and water imbibition in repair-old mortar composites", Measurement, 183, 109769, 2021. https://doi.org/10.1016/j.measurement.2021.109769

[31] Cnudde, V., Boone, M. N. "High-resolution X-ray computed tomography in geosciences: A review of the current technology and applications", Earth-Science Reviews, 123, pp. 1–17, 2013. https://doi.org/10.1016/j.earscirev.2013.04.003

[32] Dong, Y., Su, C., Qiao, P., Sun, L. "Microstructural crack segmentation of three-dimensional concrete images based on deep convolutional neural networks", Construction and Building Materials, 253, 119185, 2020. https://doi.org/10.1016/j.conbuildmat.2020.119185

[33] Lai, Z., Chen, Q. "Reconstructing granular particles from X-ray computed tomography using the TWS machine learning tool and the level set method", Acta Geotechnica, 14(1), pp. 1–18, 2019. https://doi.org/10.1007/s11440-018-0759-x

[34] Wang, P., Qiao, H., Zhang, Y., Li, Y., Feng, Q., Chen, K. "Meso-damage evolution analysis of magnesium oxychloride cement concrete based on X-CT and grey-level co-occurrence matrix", Construction and Building Materials, 255, 119373, 2020. https://doi.org/10.1016/j.conbuildmat.2020.119373

[35] Tian, W., Han, N. "Analysis on meso-damage processes in concrete by X-ray computed tomographic scanning techniques based on divisional zones", Measurement, 140, pp. 382–387, 2019. https://doi.org/10.1016/j.measurement.2019.04.026

[36] Liu, J., Jiang, R., Sun, J., Shi, P., Yang, Y. "Concrete Damage Evolution and Three-Dimensional Reconstruction by Integrating CT Test and Fractal Theory", Journal of Materials in Civil Engineering, 29(9), 04017122, 2017. https://doi.org/10.1061/(ASCE)MT.1943-5533.0001932

[37] Gan, L., Xu, W., Shen, Z., Xu, L., Zhang, W., Zhang, H., Abbas, M. A., Chen, G. "Experimental and numerical investigations on damage evolution of concrete under sulfate attack and freeze-thaw cycles", Journal of Building Engineering, 71, 106469, 2023. https://doi.org/10.1016/j.jobe.2023.106469

[38] Wang, H. C., Zhao, J., Li, J., Braithwaite, C. H., Zhang, Q. B. "Progressive fracturing of concrete under biaxial confinement and repetitive dynamic loadings: From damage to catastrophic failure", International Journal of Impact Engineering, 165, 104232, 2022. https://doi.org/10.1016/j.ijimpeng.2022.104232

[39] Xue, S., Zhang, P., Bao, J., He, L., Hu, Y., Yang, S. "Comparison of Mercury Intrusion Porosimetry and multi-scale X-ray CT on characterizing the microstructure of heat-treated cement mortar", Materials Characterization, 160, 110085, 2020. https://doi.org/10.1016/j.matchar.2019.110085

[40] Luo, Q., Zhao, L., Wu, M. "Microstructural damage characterization of NC-UHPC composite under salt freeze-thaw cycles based on ex-situ X-ray computed tomography", Construction and Building Materials, 414, 134980, 2024. https://doi.org/10.1016/j.conbuildmat.2024.134980

[41] Schock, J., Liebl, S., Achterhold, K., Pfeiffer, F. "Obtaining the spacing factor of microporous concrete using high-resolution Dual Energy X-ray Micro CT", Cement and Concrete Research, 89, pp. 200–205, 2016. https://doi.org/10.1016/j.cemconres.2016.08.008

[42] Volume Graphics "VG Studio Max (2023.1)", [computer program] Available at: https://www.volumegraphics.com/en/products/software-release/version-2023-1.html [Accessed: 31 March 2023]

[43] CEN "EN 196-1:2016 Methods of testing cement - Part 1: Determination of strength", European Committee for Standardization, Brussels, Belgium, 2016.

[44] MSZT "MSZ EN 480-11:2006 Adalékszerek betonhoz, habarcshoz és injektálóhabarcshoz. Vizsgálati módszerek. 11. rész: A megszilárdult beton légbuborék-jellemzőinek meghatározása (Admixtures for concrete, mortar and grout - Test methods - Part 11: Determination of air void characteristics in hardened concrete)", Magyar Szabványügyi Testület, Budapest, Hungary, 2006. (in Hungarian)